Plasma Science and Technology

PAPER

Fabrication and characterization of iron and iron carbide thin films by plasma enhanced pulsed chemical vapor deposition

Plasma Sci. Technol. **21** (2019) 105502 (7pp) https://doi.org/10.1088/2058-6272/ab2bbf

Fabrication and characterization of iron and iron carbide thin films by plasma enhanced pulsed chemical vapor deposition

Yulian HU (胡玉莲), **Xu TIAN** (田旭), **Qipeng FAN** (樊启鹏), **Zhengduo WANG** (王正铎), **Bowen LIU** (刘博文), **Lizhen YANG** (杨丽珍) and **Zhongwei LIU** (刘忠伟)

Laboratory of Plasma Physics and Materials, Beijing Institute of Graphic Communication, Beijing 102600, People's Republic of China

E-mail: liuzhongwei@bigc.edu.cn

Received 4 May 2019, revised 14 June 2019
Accepted for publication 20 June 2019
Published 2 August 2019

Abstract

A new pulsed chemical vapor deposition (PCVD) process has been developed to fabricate iron (Fe) and iron carbide ($Fe_{1-x}C_x$) thin films at low temperature range from 150 °C to 230 °C. The process employs bis(1,4-di-*tert*-butyl-1,3-diazabutadienyl)iron(II) as iron source and hydrogen gas or hydrogen plasma as the coreactant. The films deposited with hydrogen gas are demonstrated polycrystalline with body-centered cubic Fe. However, for the films deposited with hydrogen plasma, the amorphous phase of iron carbide is obtained. The influence of the deposition temperature on iron and iron carbide characteristics have been investigated.

Keywords: Fe and $Fe_{1-x}C_x$ films, H_2 plasma, pulsed chemical vapor deposition

(Some figures may appear in colour only in the online journal)

1. Introduction

As one of the most important earth-abundant transition metal elements, iron metal and iron carbides have many exciting and promising applications. In the catalysis area, iron demonstrates excellent catalytic performance in Fisher–Tropsch reactions [1], the Haber–Bosch process [2], wet oxidation with hydrogen peroxide [3] and carbon nanotube production [4]. Iron films have also been fabricated on GaAs semiconductor substrates to introduce the magnetic metal layer into planar electronic circuits for spintronic applications [5]. Also, iron can be used as components in metallic alloys and iron-based compounds. For example, FeNi, FeCo, FeNiCo have been applied in data storage or MEMS devices [6]. Similarly, iron carbides have attracted tremendous attention due to their unique physicochemical properties, and have been widely applied in oxygen reduction reactions [7], electrocatalysis [8], batteries [9] and supercapacitors [10].

Generally, Fe films were grown by physical vapor deposition (PVD) [11] and the wet chemical method [12], such as impregnation of metallic support materials, ion exchange, and co-crystallization. An alternative way to deposit Fe films is chemical vapor deposition (CVD) [13–16]. Compared to the PVD method, CVD is able to coat three-dimensional structures with high deposition rates and mild deposition conditions [17–21]. However, the selection of a suitable iron precursor is crucial to achieve high quality iron films in CVD processes. Over the past year, a wide range of iron precursors have been studied, including iron pentacarbonyl ($Fe(CO)_5$) [22–24], ferrocene ($FeCp_2$) [16, 24], bis(μ-carbonyl-carbonyl-η-cyclopentadienyl)iron ($Fe_2Cp_2(CO)_4$) [25], iron tri(bismethylsilyl)amid ($Fe(N(TMS)_2)_3$) [26], (1,3-butadiene)(toluene)Fe and (1,3-cyclohexadiene) (toluene)Fe [27], $H_2Fe[P(CH_3)_3]_4$ and $H_2Fe[P(OCH_3)_3]_4$ [13], bis(*N,N′*-diisopropylacetamidinate)iron(II) ($Fe_2(\mu\text{-}^{i}Pr\text{-}MeAMD)_2(\eta^2\text{-}^{i}Pr\text{-}MeAMD)_2$) and bis(*N,N′*-di-tert-butylacetamidinate)iron(II) ($Fe(^{t}Bu\text{-}MeAMD)_2$) [28, 29]. Among these precursors, $Fe(CO)_5$, $Fe_2Cp_2(CO)_4$ and $H_2Fe[P(OCH_3)_3]_4$ structures contain oxygen elements, which tend to form impurity in the films. In addition, the most often used precursor $Fe(CO)_5$ yields pure iron films at deposition temperatures of 130 °C–250 °C [14], however, it is highly

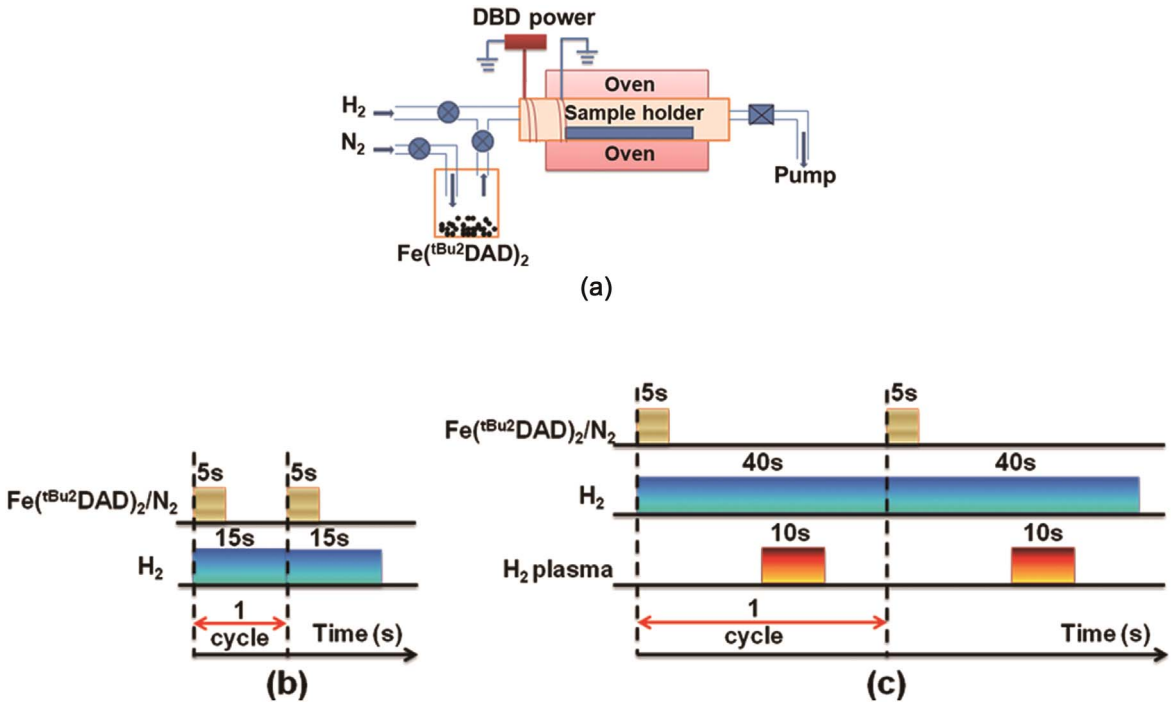

Figure 1. (a) Schematic of the tubular PCVD reactor and schematic layout of the typical cycles, (b) 5 s $Fe(^{tBu2}DAD)_2$ pulse and10 s H_2 purge, and (c) 5 s $Fe(^{tBu2}DAD)_2$ pulse, 15 s H_2 purge, 10 s H_2 plasma, and 10 s H_2 purge pulse.

toxic, flammable, and heat-, air-, and light-sensitive. (1,3-butadiene)(toluene)Fe and (1,3-cyclohexadiene) (toluene)Fe were reported to produce Fe films using He as a carrier gas with low deposition temperature down to 150 °C, but limited information was provided on the processes and film characterization [27]. Other precursors are relatively stable, but higher deposition temperature above 200 °C is needed [26, 30]. Recently, the Winter group [31] reported a new iron precursor, bis(1,4-di-*tert*-butyl-1,3diazabutadienyl)iron (II) [$Fe(^{tBu2}DAD)_2$]. Compared with other iron precursors, $Fe(^{tBu2}DAD)_2$ is easy to synthesize and purify and has high volatility at convenient temperature. In particular, $Fe(^{tBu2}DAD)_2$ is a non-oxygenated metal organic complex with ligand-metal bonding through Fe-N bonds, which avoid the oxygen impurities incorporating into the films.

The present work reports a new pulsed chemical vapor deposition process to deposit Fe and $Fe_{1-x}C_x$ films at low temperature of 150 °C–230 °C, using $Fe(^{tBu2}DAD)_2$ as the Fe source and either hydrogen gas or hydrogen plasma as a coreactant. The influences of a reducing agent and deposition temperatures on the property of pulsed chemical vapor deposition (PCVD) films have been carefully investigated.

2. Experimental

The depositions of Fe and $Fe_{1-x}C_x$ films were performed in a home-made CVD reactor, which is schematically shown in figure 1(a). The detailed configuration of the reactor can be found in our previous report [32–35], and only the main features are outlined here. The deposition chamber consists of a half-cylinder aluminum sample holder and a 60 cm long fused silica tube inside an oven that was heated up to 150 °C–230 °C ± 1 °C. A thermocouple was attached to the sample holder to give a direct measurement of the deposition temperature. Two copper coils were used as discharge electrodes, which were wrapped outside the upstream of the silica deposition chamber. The high voltage electrode was connected to the dielectric barrier discharge power supply source providing a bipolar sine wave output with 0–30 kV peak-to-peak voltage at the frequency of 30 kHz. The distance between two electrodes is 100 mm, and the sample substrates were normally placed near the grounded one. To provide adequate vapor pressure for the deposition, $Fe(^{tBu2}DAD)_2$ precursor was maintained at 90 °C and then delivered into the reactor using pure nitrogen (99.999%) gas as a carrier gas with the flow rate at 50 sccm during the precursor feed time. Pure hydrogen gas (99.999%) and hydrogen plasma were employed as the coreactant for Fe and $Fe_{1-x}C_x$ deposition, respectively. The flow rate of hydrogen was kept at 50 sccm. Hydrogen plasma was generated between two electrodes. In the PCVD process, the iron precursor was delivered in a pulsed manner, instead of a continuous one, as in the CVD technique. In our case, the $Fe(^{tBu2}DAD)_2$ precursor exposure time was fixed at 5 s while hydrogen was introduced into the reactor chamber continuously. The PCVD cycles are shown schematically in figures 1(b) and (c). For the deposition using hydrogen plasma, the typical deposition recipe contained 5 s $Fe(^{tBu2}DAD)_2$ pulse, 15 s hydrogen purge, 10 s hydrogen plasma, 10 s hydrogen pulse in sequence, and the discharge voltage was about 11.4 kV. Glass slides and Si (100) wafers were used as the deposition substrates for studying the deposition behavior, and no appreciable difference was observed. Generally, Si (100) wafers were used as sample

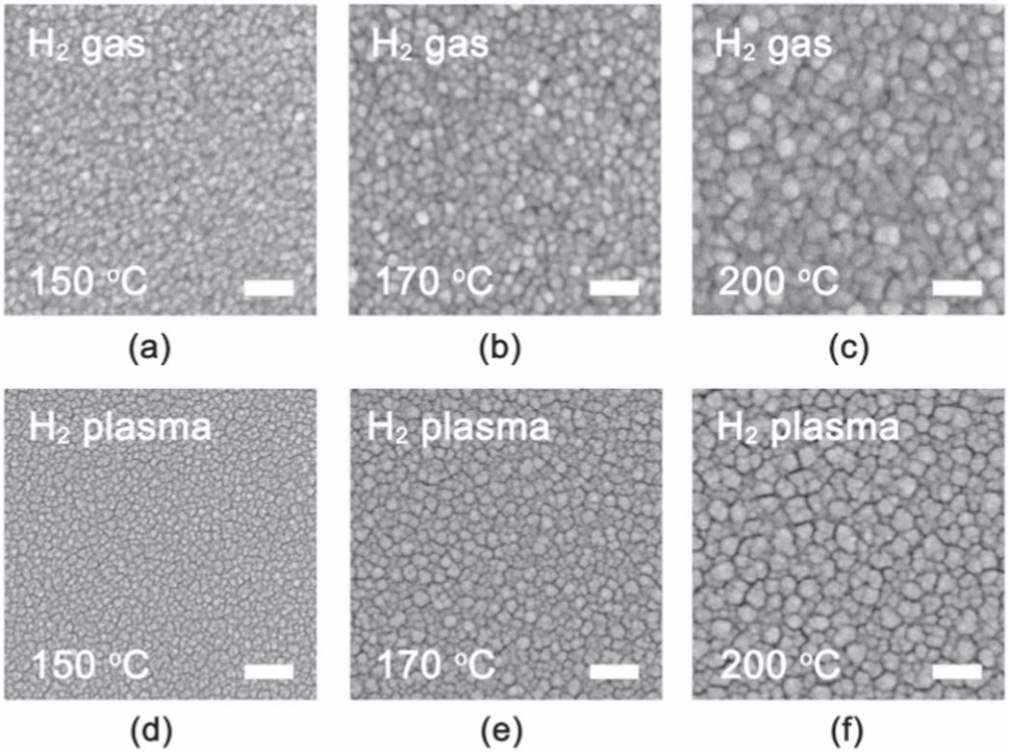

Figure 2. SEM top-view images of the 300-cycle films deposited on Si substrates with (a)–(c) H_2 gas or (d)–(f) H_2 plasma at various different temperatures. The scale bars stand for 100 nm.

Table 1. Thicknesses (nm) of the 300-cycle films deposited on glass slide substrates with H_2 gas or H_2 plasma at various different temperatures.

Deposition condition	Temperature (°C)			
	150	170	200	230
H_2 gas	60.5	83.2	89.6	87.3
H_2 plasma	66.4	88.3	90.1	89.4

substrates for SEM, XPS measurements and glass slides for film thickness and XRD analysis. Prior to the deposition, the substrates were sequentially rinsed with acetone, methanol, and isopropanol, and then pretreated by 1 min of H_2 plasma.

The deposited PCVD films were firstly scratched and then measured the step profiles (Veeco, Dektak 150) across the scratched lines to obtain the thickness. The surface morphology of the films was investigated by a scanning electron microscopy (SEM) (Hitachi, SU8020). The X-ray photoelectron spectroscopy (XPS) (Thermo Scientific, K-Alpha) was used to determine the composition of the films. The X-ray diffraction (XRD) (Rigaku, D/max-2200 PC) was taken to evaluate the crystalline structure of deposited films. The microstructure of deposited films was analyzed by transmission electron microscopy (TEM) (JEOL, JEM2100). The Raman spectrometer (Titan, RTS-2) with the excitation wavelength of 532 nm was used to acquire the Raman spectra. Sheet resistance measurements were carried out using a four-point probe station (RTS-8).

3. Results and discussion

The thickness of 300-cycle deposited films using H_2 gas or H_2 plasma as the reducing agent was carefully investigated at the temperature range from 150 °C to 230 °C, as shown in table 1. With a deposition recipe of 5 s $Fe(^{tBu2}DAD)_2$ pulse and continuous hydrogen gas, the thickness increased from 60.5 nm to 88.6 nm as the deposition temperature was raised from 150 °C to 200 °C. As the deposition temperature was beyond 200 °C, the thicknesses of the PCVD films remained relatively constant. When the hydrogen plasma was switched on, the deposition rate was slightly higher than that of hydrogen gas. A commonly known fact is that the plasma shows a positive effect on the thin film growth rate due to the high reactivity of the plasma [36]. Generally, the plasma consists of various reactive species, such as ions, photons, electrons, radicals and excited species [37, 38]. These active species are able to create reactive surface sites with a higher density, resulting in the larger growth rate.

Figure 2 shows the surface morphology of 300-cycle films deposited with H_2 or H_2 plasma at temperature ranging from 150 °C to 200 °C. Continuous and smooth films were observed from entire substrates. The grain size of the film deposited with H_2 gas increases from 24 nm to 45 nm with increasing deposition temperatures from 150 °C to 200 °C. For films grown with H_2 plasma, the grain size shows similar increasing tendency with raising the deposition temperature. Note that the temperature effect was especially enhanced for deposition conditions performed at 200 °C. This could be

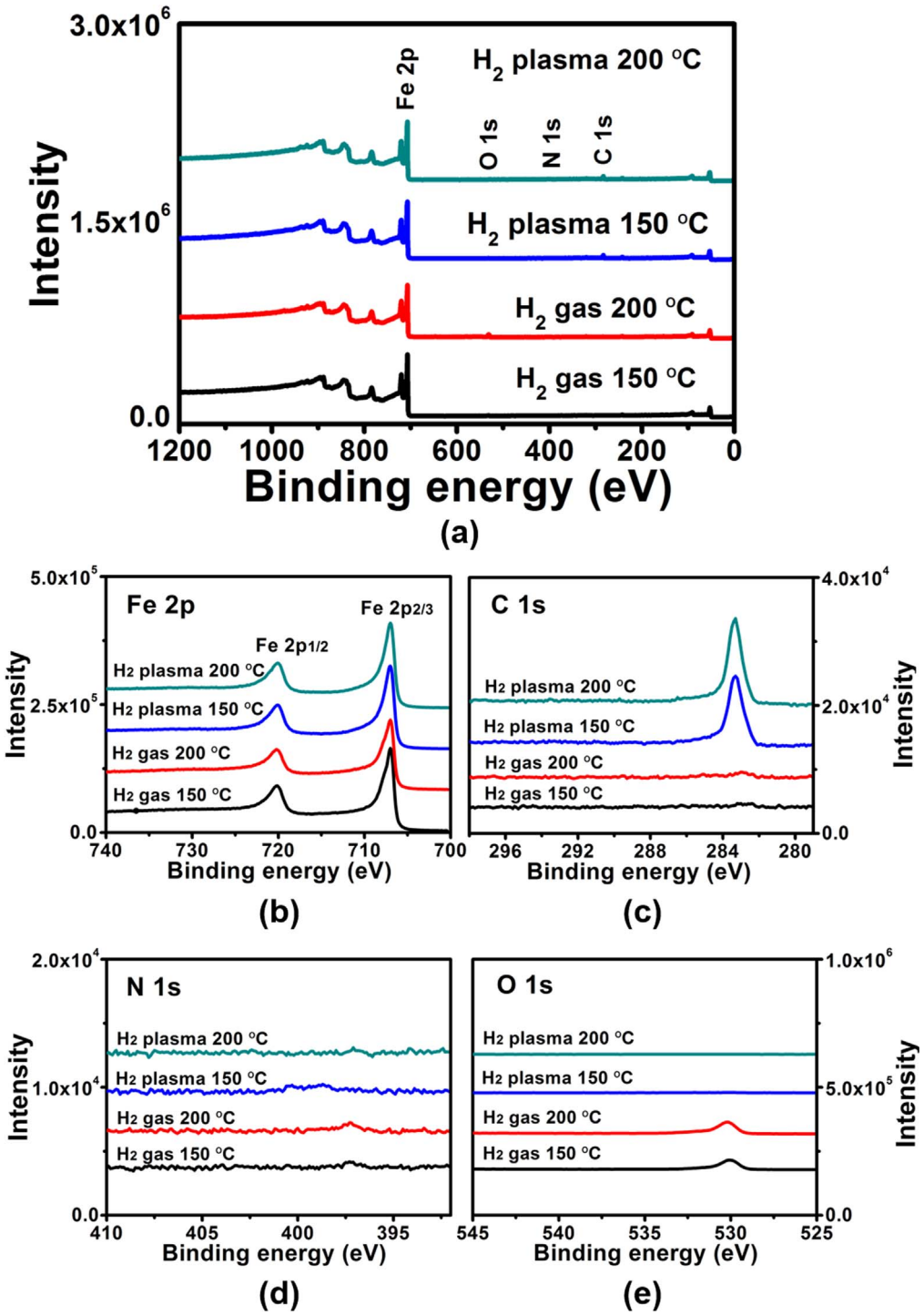

Figure 3. XPS surveys (a) and high-resolution spectra of the (b) Fe 2p, (c) C 1s, (d) N 1s and (e) O 1s core-level emissions for the films deposited with H_2 gas or H_2 plasma at 150 °C and 200 °C.

ascribed to the accelerated diffusivity for surface atom at high deposition temperature.

The element composition of the deposited films was examined by XPS. All the samples were measured after 80 s Ar^+ sputtering to removing the surface oxide and adventitious carbon. The spectra for the 300-cycle films deposited with H_2 gas or H_2 plasma at 150 °C and 200 °C were shown in figure 3. The spectra for deposition temperature at 170 °C exhibit generally the same features, so they are not shown here, but table 2 lists all films analysis results. The survey spectra of PCVD films (figure 3(a)) show the peaks from C and Fe photoelectron emissions. High-resolution spectra was used to detect Fe 2p, C 1s, N 1s, and O 1s, respectively, as shown in figures 3(b)–(e). Basing on the peak areas for the spectrum, the corresponding atomic concentrations of elements were listed in table 2. For the films grown with H_2 gas, Fe contents are above 94 at%, and the amounts of nitrogen and carbon are below the XPS detection limit of ∼1 at%. The

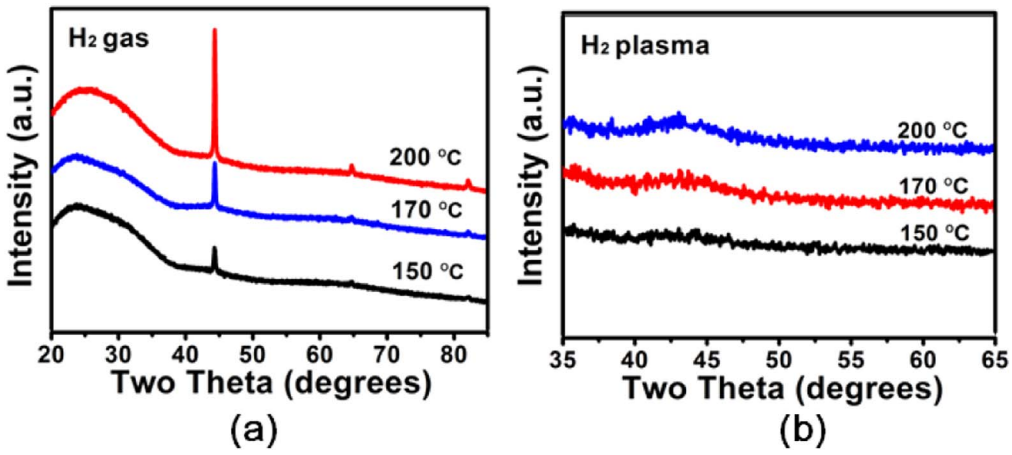

Figure 4. XRD results for films deposited on glass slide substrates using (a) H_2 gas or (b) H_2 plasma as the reducing agent at various temperatures.

Table 2. Elemental composition of the 300-cycle PCVD films deposited on Si substrates with H_2 gas or H_2 plasma at various different temperatures.

Coreactant	Temperature (°C)	Fe (at%)	C (at%)	N (at%)	O (at%)
H_2 gas	150	95.9	0.8	0.2	3.1
	170	94.8	1.1	0.2	3.9
	200	94.1	1.5	0.1	4.3
H_2 plasma	150	75.3	23.9	0.2	0.6
	170	74.8	24.2	0.1	0.9
	200	74.6	24.3	0.1	1.0

3–5 at% oxygen contents can be attributed to the post oxidation of Fe thin film by air, since there is no oxygen in the precursor molecules and no external oxygen source is provided. Actually, iron has extreme reactivity to water and oxygen, particularly in the case of nanoscale iron. In contrast, for the films deposited with H_2 plasma, the amounts of carbon were as high as ~24 at%. If we analyzed carefully the Fe XPS spectra (figure 3(b)), the binding energies of Fe $2p_{3/2}$ for the films deposited using H_2 gas or H_2 plasma were all found at 707.0 eV, which is consistent with previous reports [39]. In addition, the C 1s spectra (figure 3(c)) of the films deposited with H_2 plasma show single peaks at 283.3 eV, which indicates the formation of $Fe_{1-x}C_x$ [39, 40]. These results suggest that H_2 plasma plays an important role in the formation of iron carbide. In the case of H_2 gas, $Fe(^{tBu2}DAD)_2$ was thermally decomposed to form pure Fe metal and the volatile diazadienyl byproduct. In contrast, the diazadienyl ligands were likely decomposed by H_2 plasma to generate C_xH_y species for the deposition with H_2 plasma. Then these active C_xH_y species react with Fe to form $Fe_{1-x}C_x$. This phenomenon has also been found in our previous study for CVD Ni and Ni_3C_x [41]. Another point worth mentioning is oxygen impurities in the films deposited with H_2 plasma decreases to the detection limit of 1 at%, indicating that $Fe_{1-x}C_x$ has a better antioxidant property compared with pure Fe.

The crystallinity of film deposited on glass slide substrate was examined by XRD. As shown in figure 4(a), all 300-cycle films deposited with H_2 gas at various temperatures exhibited crystalline diffraction peaks centered at 44.67°, 65.10° and 82.33°, which can be respectively assigned to the (110), (200) and (211) planes of Fe (PDF#06-0696). Application of the Scherer law gave a mean crystallite size of 25.9 nm in the temperature range of 150 °C–200 °C. For the films deposited with H_2 plasma, no obvious reflection was observed except for a broad peak centered at 43°, indicating that the as-deposited films are mainly amorphous. This observation is similar to the results reported by Furlan [39]. $Fe_{1-x}C_x$ is a weak carbide forming metal in which the carbon content has a significant effect on its structure. As the amount of carbon exceeds 20%, amorphous $Fe_{1-x}C_x$ films tend to be formed [42]. Another important factor is the deposition temperature. As Tajima and Hirano reported [43], amorphous $Fe_{1-x}C_x$ films were fabricated via the technique of radio frequency magnetron sputtering at 250 °C. As the deposition temperature was elevated to 400 °C, the crystalline with a mixture of Fe and Fe_3C was obtained. In this work, the carbon contents of the deposited $Fe_{1-x}C_x$ films are ~24% with the deposition temperature ranging from 150 °C to 200 °C. So the resultant films are amorphous, which will be confirmed from the following TEM image (figure 5).

The corresponding high magnification TEM image and electron diffraction (ED) pattern were further used to investigate the microstructures of PCVD films at 150 °C. As shown in figure 5(a), the films with H_2 gas were polycrystalline and the grain size is around 25 nm, which was in agreement with the XRD results. Figure 5(c) shows the corresponding

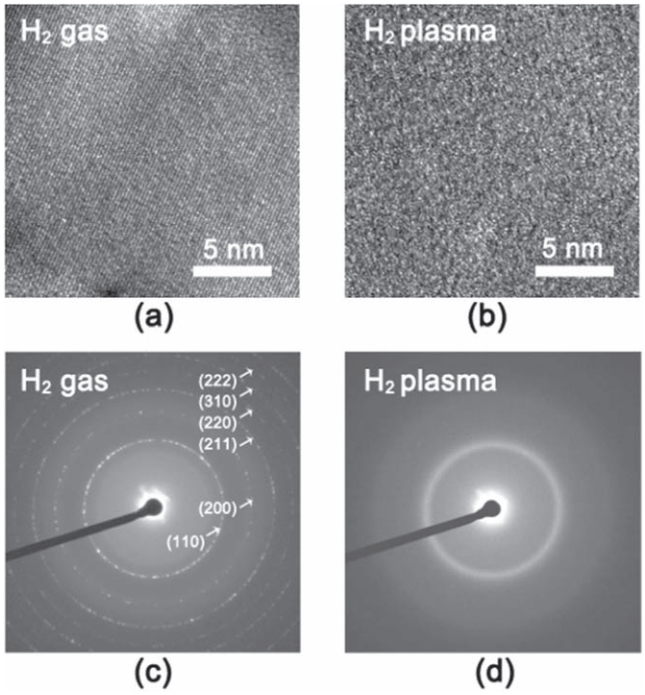

Figure 5. TEM images (a), (b) and the corresponding ED patterns (c), (d) for the films deposited with (a), (c) H_2 gas or (b), (d) H_2 plasma as the reducing agent at 150 °C.

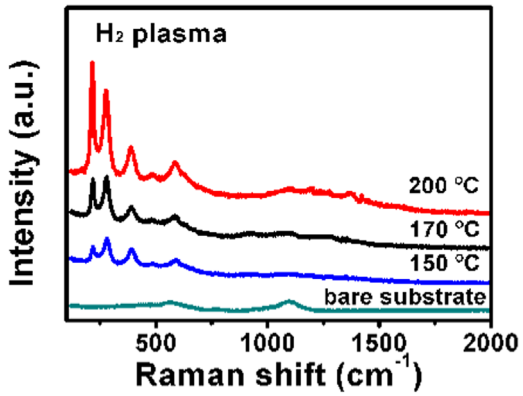

Figure 6. Raman spectra for the films deposited on glass slide substrates using H_2 plasma at different temperatures.

electron diffraction pattern. Clear diffraction rings can be observed, which agreed well with the body centered cubic (bcc) Fe (PDF#06-0696) as previously determined from XRD. However, if the reducing agent instead used H_2 plasma, no lattice fringes and diffraction rings can be observed. Thus, the film grown with H_2 plasma was again proven to be amorphous.

Figure 6 shows Raman spectra of the films deposited with H_2 plasma at various different temperatures ranging from 150 °C to 200 °C. For comparison purposes, the Raman spectrum for the substrate of glass slide has also been depicted as the reference. All curves shown in figure 6 display broad bands centered at ~570 cm^{-1} and 1100 cm^{-1}, which can be assigned to Si–O–Si of glass slide substrates. Peaks in the range of 200–500 cm^{-1} can be ascribed to the iron carbide. These results are consistent with data presented by Zhao and Prandhan [44, 45].

Table 3. Resistivities ($\mu\Omega$ cm) of the 300-cycle films deposited on glass slide substrates with H_2 gas or H_2 plasma at various different temperatures with the value uncertainty ±5%.

Deposition condition	Temperature (°C)			
	150	170	200	230
H_2 gas	72	85	88	92
H_2 plasma	358	367	372	376

Table 3 represents the resistivity of the 300-cycle films produced using H_2 gas or H_2 plasma as the reducing agent. With increasing the deposition temperature from 150 °C to 230 °C, the resistivity of the films grown with H_2 gas increased slightly from 72 $\mu\Omega$ cm to 92 $\mu\Omega$ cm, which was very close to that for a sputtered Fe film (70 $\mu\Omega$ cm) [36]. For films deposited with H_2 plasma, a similar increasing trend was observed. However, the resistivity values of films using H_2 plasma were almost four times larger than those for H_2 gas. This dramatic increase very likely comes from the change of C contents of the deposited films. As mentioned previously, the film crystal phase changes from Fe to amorphous $Fe_{1-x}C_x$, the C content increased from low (1.2–2.0 at%) to high level (~24 at%).

4. Conclusions

A pulsed chemical vapor deposition process has been developed to deposit Fe and $Fe_{1-x}C_x$ thin films. At a certain experimental condition (5 s $Fe(^{tBu2}DAD)_2$ pulse with continuous H_2 gas, the deposition temperature range 150 °C–230 °C), pure and continuous Fe films were obtained. When H_2 plasma was used as a coreactant instead of H_2 gas, amorphous iron carbide films were deposited. The results show that this PCVD process can be applicable to tune the elemental composition of Fe-based compounds and extend to fabricate other transition metal compounds.

Acknowledgments

This work is financially supported by National Natural Science Foundation of China (No. 11775028), Collaborative Innovation Center of Green Printing & Publishing Technology (No. 15208) and Beijing Institute of Graphic Communication Project (Nos. Ea201801 04190119001-020 and 12000400001).

References

[1] Yang J *et al* 2014 *Appl Catal. A: Gen.* **470** 250
[2] Hu L K *et al* 2018 *ACS Catal.* **8** 9312
[3] Centi G *et al* 2000 *Catal. Today* **55** 61

[4] Lee K S *et al* 2012 *Int. J. Hydrogen Energy* **37** 6268
[5] Haugan H J *et al* 2002 *J. Magn. Magn. Mater.* **247** 296
[6] Zhang P Y *et al* 2015 *J. Vac. Sci. Technol.* A **33** 061521
[7] Fan X J *et al* 2015 *ACS Nano* **9** 7407
[8] Jiang H L *et al* 2015 *ACS Appl. Mater. Interfaces* **7** 21511
[9] Paulraj A R *et al* 2017 *J. Electrochem. Soc.* **164** A1665
[10] Vermisoglou E C *et al* 2014 *J. Alloys Compd.* **590** 102
[11] Weston W F *et al* 1978 *J. Vac. Sci. Technol.* **15** 54
[12] Hong X L *et al* 2014 *Thin Solid Films* **589** 649
[13] Park S 2006 *Chem. Mater.* **18** 5150
[14] Aviziotis I G *et al* 2017 *Adv. Mater. Interfaces* **4** 1601185
[15] Krisyuk V *et al* 2010 *J. Electrochem. Soc.* **157** D454
[16] Lubej M and Plazl I 2014 *Chem. Eng. J.* **242** 306
[17] Zhao R and Wang X W 2019 *Chem. Mater.* **31** 445
[18] Guo Z and Wang X W 2018 *Angew. Chem. Int. Ed.* **57** 5898
[19] Li H *et al* 2017 *J. Mater. Chem.* A **5** 21353
[20] Li H *et al* 2015 *Nano Lett.* **15** 6689
[21] Xiong W *et al* 2017 *ACS Energy Lett.* **2** 2778
[22] Walsh P J and Bottka N 1984 *J. Electrochem. Soc.* **131** 444
[23] Lane P A and Wright P J 1999 *J. Cryst. Growth* **204** 298
[24] Senocq F *et al* 2006 *J. Electrochem. Soc.* **153** G1025
[25] Feurer R *et al* 1988 *Thin Solid Films* **167** 195
[26] Baxter D V *et al* 1995 *Chem. Vap. Deposition* **1** 49
[27] Michkova K *et al* 2006 *Appl. Catal. A: Gen.* **315** 83
[28] Gleizes A N *et al* 2009 *ECS Trans.* **25** 181
[29] Lim B S, Rahtu A and Gordon R G 2003 *Nat. Mater.* **2** 749
[30] Stauf G T *et al* 1987 *Thin Solid Films* **153** 421
[31] Knisley T J *et al* 2011 *Organometallics* **30** 5010
[32] Guo Z *et al* 2015 *Chem. Mater.* **27** 5988
[33] Guo Q *et al* 2018 *ACS Appl. Mater. Interfaces* **10** 8384
[34] Xiong W *et al* 2018 *J. Mater. Chem.* A **6** 4297
[35] Fan Q P *et al* 2019 *J. Vac. Sci. Technol.* A **37** 010904
[36] Xu Z J *et al* 2013 *Adv. Mater. Res.* **690–693** 1664
[37] Chen Q and Ichiki T 2015 *Plasma Sources Sci. Technol.* **24** 025022
[38] Chang X H *et al* 2018 *Nano Res.* **11** 2724
[39] Furlan A *et al* 2015 *J. Phys.: Condens. Matter* **27** 045002
[40] Lu Y W *et al* 2017 *Fuel* **193** 369
[41] Guo Q *et al* 2018 *MRS Commun.* **8** 88
[42] Bauer-Grosse E and Aouni A 2007 *J. Non-Cryst. Solids* **353** 3644
[43] Tajima S and Hirano S 1993 *J. Mater. Sci.* **28** 2715
[44] Wang H H *et al* 2017 *Rsc Adv.* **7** 3921
[45] Pradhan S *et al* 2007 *Metall. Mater. Trans.* A **38** 2363